Chemical Geology 606 (2022) 120995

Contents lists available at ScienceDirect

Chemical Geology

journal homepage: www.elsevier.com/locate/chemgeo

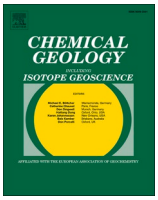

Hematite-goethite ratios at pH 2–13 and 25–170 °C: A time-resolved synchrotron X-ray diffraction study

Si Athena Chen [a,*], Peter J. Heaney [a], Jeffrey E. Post [b], Peter J. Eng [c,d], Joanne E. Stubbs [c]

[a] Department of Geosciences, Penn State University, University Park, PA 16802, United States of America
[b] Department of Mineral Sciences, Smithsonian Institution, Washington, D.C. 20560, United States of America
[c] Center for Advanced Radiation Sources, The University of Chicago, Chicago, IL 60637, United States of America
[d] James Franck Institute, The University of Chicago, Chicago, IL 60637, United States of America

ARTICLE INFO

Editor: Hailiang Dong

Keywords:
Hematite
Goethite
2-line Ferrihydrite
Iron Oxides
Time-resolved X-ray diffraction

ABSTRACT

Iron (oxyhydr)oxides are sensitive indicators of pH, Eh, temperature, microbial activity, and climate conditions in the Critical Zone. The most ubiquitous and environmentally significant iron oxides in most soils are two-line ferrihydrite, goethite, and hematite. Here we present a comprehensive study of the transformation of two-line ferrihydrite to hematite and goethite over a wide range of temperature (25–170 °C) and initial pH (2–13) conditions through *ex situ* batch and *in situ* synchrotron X-ray diffraction (XRD) experiments.

Within the high time resolution of our experiments, goethite and hematite nucleated nearly simultaneously from ferrihydrite in nearly equal concentrations by mass. Hematite increased in abundance relative to goethite until a steady-state ratio was achieved, and both phases ceased growth on the depletion of ferrihydrite. Higher temperatures and lower water activities favored hematite formation at all pH values studied. In both our batch and our time-resolved, angle-dispersive synchrotron X-ray diffraction experiments, hematite was favored relative to goethite at an initial pH of 3 to 5. In contrast, goethite preferentially formed in neutral (initial pH 7–8) and highly alkaline conditions (initial pH ≥ 11). Surprisingly, mildly alkaline conditions (initial pH 9–11) induced the precipitation of a highly Fe-deficient (Fe_{occ} = ~0.80–0.90) variety of hematite known as "hydrohematite" in greater concentrations than goethite. Our results are useful for the application of hematite-goethite ratios as paleoclimate proxies for soil and sediment systems with low pH buffering capacities.

1. Introduction

Two-line ferrihydrite (referred to as ferrihydrite below), with an approximate formula of $Fe^{3+}_{10}O_{14}(OH)_2$, is a poorly crystalline and metastable iron oxyhydroxide that frequently occurs in aqueous environments, such as in hydromorphic soils, rock-drainage waters, groundwaters, and marine environments (Carlson and Schwertmann, 1981; Childs, 1992; Jambor and Dutrizac, 2003; Michel et al., 2007). In many soil systems, ferrihydrite transforms to the thermodynamically favored Fe (oxyhydr)oxides goethite (α-FeOOH) and hematite (α-Fe_2O_3), typically over short timescales (Paterson, 1999; Lagroix et al., 2016). Because of the ubiquity of Fe (oxyhydr)oxides in the Critical Zone, understanding the kinetics and mechanisms by which this transformation occurs can yield insights into weathering processes on Earth and Mars (Christensen et al., 2001; Fraeman et al., 2013; Chen et al., 2021). The three most significant factors that influence the extent of transformation are pH, temperature, and time (Schwertmann and Murad, 1983; Das et al., 2011; Colombo et al., 2014; Lagroix et al., 2016). Although this transformation has been extensively studied, the variable ratios of hematite to goethite in the reaction products have been reported for only limited pH and temperature conditions (Vu et al., 2010; Das et al., 2011).

The relative concentrations of hematite and goethite often are quantified through the "hematite-goethite ratio", which is calculated as the wt% hematite/(wt% hematite + wt% goethite) in a mixture. This ratio has been used as a pedoenvironmental indicator for water precipitation (Hyland et al., 2015; Long et al., 2016), global warming (Lagroix et al., 2016), landscape dissection (Silva et al., 2020), and soil relief (Camargo et al., 2013). Moreover, the relative concentrations of hematite and goethite in soils have significant implications for metal

Abbreviations: Hm, Hematite; Gt, Goethite; Fh, Ferrihydrite; Hyhm, Hydrohematite; XRD, X-ray diffraction.

* Corresponding author.
E-mail addresses: siathenachen@gmail.com (S.A. Chen), pjheaney@psu.edu (P.J. Heaney).

https://doi.org/10.1016/j.chemgeo.2022.120995
Received 7 December 2021; Received in revised form 13 June 2022; Accepted 16 June 2022
Available online 20 June 2022

adsorption, ion exchange, catalytic activity, magnetic properties, microbial activity, and physical properties (such as color and shear strength) of soil systems (Carlson and Schwertmann, 1981; Childs, 1992; Cornell and Schwertmann, 2003; Ferris, 2005; Vu et al., 2010; Parry, 2011). As hematite and goethite are abundant not only in nature but also are important industrial materials, knowledge of the hematite-goethite ratio under various synthesis conditions offers important technological implications as well (Schwertmann and Cornell, 1992; Cornell and Schwertmann, 2003).

Generally, hematite forms preferentially to goethite at higher temperatures, lower moisture conditions, and with less organic matter, but the relationship with pore solution pH is more complicated (Kämpf and Schwertmann, 1983). Many studies have indicated that the hematite-goethite ratio has a high sensitivity to pH (Johnston and Lewis, 1983; Schwertmann and Murad, 1983; Ocaña et al., 1995; Das et al., 2011). Schwertmann and his coauthors first quantitatively studied the transformation of two-line ferrihydrite at low temperatures (4–25 °C) and pH 2.5–12 up to 10–12 years with pH adjustments every several months (Schwertmann and Murad, 1983; Schwertmann et al., 1999, 2004). Using XRD and Mössbauer spectra, their results showed that hematite formation was maximized between pH 7 and 8, whereas goethite dominated at pH 4 and pH 12.

More recent studies, using novel *in-situ* synchrotron XRD techniques, have advanced the study of iron oxide transformations to a time-resolution of minutes (Shaw et al., 2005; Vu et al., 2010; Brinza et al., 2015; Peterson et al., 2018). However, some of these investigations employed energy- rather than angle-dispersive approaches, inhibiting the application of whole-pattern analysis by Rietveld methods (Shaw et al., 2005; Vu et al., 2010; Brinza et al., 2015). Moreover, these studies focused on Fe (oxyhydr)oxide transformations at a specific initial pH: 1.4 (Peterson et al., 2018), 8 (Brinza et al., 2015), 10.7 (Shaw et al., 2005), and 13.2 or higher (Shaw et al., 2005; Vu et al., 2010). No studies have interrogated ferrihydrite transformations with a time resolution of seconds and over a range of pH concentrations, temperatures, and time.

In the present work, we highlight the transformation of ferrihydrite to hematite and goethite over a wide range of unbuffered, initial pH (2−11) and at temperatures from 25 to 170 °C. In addition, we performed both *in vitro* batch experiments and *in situ* time-resolved experiments, using two-line ferrihydrite synthesized in static systems from unbuffered iron nitrate solutions without seeding. We monitored crystal growth after setting the initial pH without additional adjustments in order to avoid the dilution that would occur during long-term experiments and to remove possible interferences between the buffers and the precipitation of hydrous phases (Ling et al., 2015). In parallel, we captured the transformation pathway in real-time by angle-dispersive time-resolved X-ray diffraction (TRXRD). The application of Rietveld analysis to our TRXRD data revealed the ratios of hematite to goethite with high time resolution, allowing us to correlate the evolution of crystal structure with pH, temperature, and reaction kinetics.

2. Materials and methods

2.1. Batch experiments

Ferrihydrite gels were prepared according to protocols modeled after those of Schwertmann and Cornell (1992) and Das et al. (2011). 0.2 *M* Fe$(NO_3)_3$ solutions were prepared by dissolving 0.20 g of $Fe(NO_3)_3 \bullet 9\,H_2O$ (Sigma-Aldrich, ACS reagent, ≥98%) in 25 mL deionized (DI) water. 1 *M* KOH solutions were prepared by dissolving 14.03 g of KOH (Sigma-Aldrich, anhydrous, ≥99.95% trace metals basis) in 250 mL DI water. 25 mL volumes of 0.2 *M* $Fe(NO_3)_3$ solutions were then titrated with 1 *M* KOH drop by drop to the initial pH of interest, ranging from 2 to 12. Brown ferrihydrite precipitated as soon as the titration started, and the viscosity of the ferrihydrite gel increased with higher pH as more ferrihydrite precipitated. The amounts of the 1 *M* KOH solutions used to titrate to each target pH are summarized in Table S1. Two-line ferrihydrite formed as soon as KOH titrated the iron nitrate solutions, as ascertained by XRD data. Each ferrihydrite gel was immediately transferred to a perfluoroalkoxy alkane (PFA) digestion vessel and sealed.

For *ex-situ* batch heating experiments between 70 °C and 170 °C, 25 mL of fresh ferrihydrite gel (with <4 h of aging at room temperature) were heated in digestion vessels in a drying oven at temperatures 70, 80, 100, 110, 130, 150, and 170 °C. After 48 h of heating, the digestion vessels were removed from the oven and cooled gradually to room temperature. We then recorded the pH of the solution at room temperature. Since the pH changed during the transformation, the "pH" designated for each run refers to the initial pH only. The changes in pH are shown in the Supporting Information (Table S2). Reaction products were filtered using 0.05 μm membranes, washed with deionized water three times, air-dried overnight in a fume hood, and weighed. Weights of final products are shown in Fig. S1.

For the *ex-situ* room temperature (RT) batch experiments, 100 mL of 0.2 *M* $Fe(NO_3)_3$ solutions were titrated with 1 *M* KOH to the initial pH of interest. The ferrihydrite gels at initial pH 2–11 were stored at a constant-temperature of 25 °C for 40 to 1517 days. We extracted 10 mL of the gels at 40, 300, 1240, and 1517 days. The changes in pH are shown in Table 1 and in the Supporting Information (Table S3). All pH measurements were conducted at room temperature. The reaction products were filtered using 0.05 μm membranes, washed with deionized water three times, air-dried overnight in a fume hood, and investigated using synchrotron XRD (Fig. S2).

2.1.1. X-ray diffraction of batch reaction products

Both conventional and synchrotron XRD were used to characterize and quantify the reaction products in the batch experiments. Once a powder had dried, it was disaggregated with acetone in an agate mortar and pestle. The powder was then placed within a polyimide (Kapton) capillary (outer diameter 0.8 mm). For the reaction products at $T \geq$ 90 °C, XRD data were collected with a Rigaku DMAX-Rapid II microdiffractometer at 50 kV and 40 mA using a Mo source (λ = 0.7107 Å) (Department of Mineral Sciences, US National Museum of Natural History). Samples were scanned from 4° to 44° 2θ at 2 °/min and rotated 180° about phi (parallel to the length of the capillary) to minimize preferred orientation. Diffraction rings were collected with an area detector, and the integration step size was 0.02°. Due to the low concentration of crystalline material in the Fe-rich mixture, for the reaction products at 70 and 80 °C, *ex-situ* synchrotron XRD data were collected at the GeoSoilEnviroCARS (GSECARS) 13-BM-C beamline at the Advanced Photon Source (APS), Argonne National Laboratory (ANL). The X-ray wavelength was 0.8266(2) Å, and the distance from beam center to sample was 96.415 mm. To reduce preferred orientation effects, the capillary was rotated from 0 to 30° about phi during a 30 s exposure time. Diffraction rings were collected using an area detector, and 2-dimensional diffraction patterns were obtained by the integration of

Table 1
Changes in pH during the transformation of ferrihydrite to hematite (Hm) and goethite (Gt).

Initial Solution pH	Temperature (80 °C), 48 h		Temperature (130 °C), 48 h	
	Final Solution pH	Hm/(Hm + Gt) (wt%)	Final Solution pH	Hm/(Hm + Gt) (wt%)
2.00(3)	1.16(1)	0.765(5)	0.68(1)	1.000(1)
3.00(3)	2.28(1)	1.000(1)	1.69(1)	1.000(1)
4.00(4)	2.23(2)	1.000(1)	1.37(2)	1.000(1)
5.00(2)	2.47(2)	0.784(5)	1.94(2)	0.901(2)
6.00(4)	4.38(2)	0.450(8)	2.20(2)	0.545(1)
7.00(3)	7.51(3)	0.388(9)	2.46(2)	0.634(6)
8.00(9)	8.14(4)	0.576(6)	6.49(3)	0.635(2)
9.00(4)	9.90(1)	0.790(2)	11.35(1)	0.886(2)
10.00(4)	11.87(1)	0.809(2)	11.92(2)	0.852(2)
11.00(4)	12.30(2)	0.369(3)	12.24(2)	0.344(2)

diffraction rings using Dioptas (Prescher and Prakapenka, 2015). All XRD patterns were analyzed using the JADE Pro v8.5 software (ICDD, Livermore, CA).

2.2. In situ, time-resolved synchrotron X-ray diffraction (TRXRD) experiments

2.2.1. Sample preparation for TRXRD experiments

Analogously to our batch experiments, fresh 1 *M* $Fe(NO_3)_3$ solutions were prepared by dissolving 40.39 g $Fe(NO_3)_3 \bullet 9\ H_2O$ in 100 mL DI water, and fresh 5 *M* KOH was prepared by dissolving 28.05 g of KOH in 100 mL DI water. Starting ferrihydrite gels for the TRXRD experiments were prepared by titrating 10 mL of 1 *M* $Fe(NO_3)_3$ solutions with 5 *M* KOH until the initial pH of interest was achieved. The volumes of KOH consumed to achieve the initial pH are presented in Supplementary Information (Table S4). The ferrihydrite gel was then injected into a 1.00 mm thin-walled quartz glass capillary (Charles Supper Company) using a syringe. The approximate volume of the ferrihydrite gel in each capillary was 0.04 mL. Capillaries were sealed using a UV fast-curing epoxy (Product #OG142–87, Epo-Tek) and a full-spectrum UV lamp (EXFO X-Cite Series 120) for 10 min. X-ray diffraction and heating and of the ferrihydrite gels were performed within 3 h of the time of injection into the capillaries to keep the ferrihydrite fresh. Solution volumes, headspaces of each capillary, UV epoxy curing time, and ferrihydrite aging time were as similar as possible to maintain consistency among samples. The starting pH concentrations for the ferrihydrite gels ranged from 2 to 13. For the TRXRD experiments, no pH buffer was added to maintain the pH. Because of the limited time available for synchrotron data collection, the TRXRD experiments were conducted only at 130 °C to maximize reaction rates.

2.2.2. Data collection conditions for time-resolved synchrotron X-ray diffraction

The TRXRD experiments were conducted at the GSECARS 13-BM-C beamline at the APS (Fig. 1). Each capillary was mounted on a goniometer and heated with a He forced-gas heater designed and fabricated at GSECARS, as described in Chen et al. (2021). The temperature was calibrated by monitoring two phase transformations of $RbNO_3$ (Alfa Aesar, 99.8%, metals basis) loaded in the same type of thin-walled quartz capillary. Based on this standardization, the temperature measured by the thermocouple was within ±1.5 °C of the actual temperature. The heater raised the temperature from 22 °C to 130 °C within 10 s and then remained at 130 °C within ±0.1 °C.

A LaB_6 SRM 660 standard (NIST) was used to determine the X-ray wavelength, the sample-to-detector distance, and the beam center position. The X-ray wavelength for the TRXRD experiments was 0.8289(4) Å, and the sample-to-detector distance was 108.51 mm. The X-ray beam was focused on the center of the heating window with a beam size of 0.3 mm in height and 0.4 mm in width (along the capillary length). Capillaries were slightly tilted at a 30° angle relative to the horizontal to promote downward sedimentation of the precipitates. Preferred orientation was minimized by rotating capillaries about phi from 0° to 30° at a rate of 1°/s. The exposure time for each pattern was 30 s.

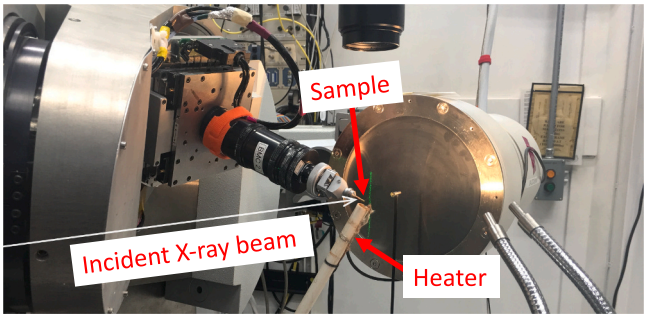

Fig. 1. Setup for time-resolved X-ray diffraction experiments at GSECARS 13-BM-C, beamline at the Advanced Photon Source, Argonne National Laboratory.

2.3. Rietveld structure refinement

Each powder pattern was fit using the General Structures Analysis System I (GSAS I) program (Larson and Von Dreele, 2000; Toby, 2001). The starting structure parameters for hematite (space group $R\bar{3}c$) and goethite (space group *Pnma*) were derived from Blake et al. (1966) and Gualtieri and Venturelli (1999), respectively. Background, scale factor, zero shift error, unit-cell, and peak profile parameters were allowed to refine. The background was fitted with a shifted Chebyshev polynomial with 12 coefficients. The large amorphous scattering humps from the capillary and water were fit as part of the background. Peak profiles were modeled using a pseudo-Voigt function with constant values for the Cagliotti peak profile functions GU, GV, and GW as determined from the refinement of a LaB_6 standard that was analyzed using the same experimental protocols as the Fe (oxyhydr)oxide samples. Profile parameters sensitive to crystal size broadening (*LX*), strain broadening (*LY*), anisotropic crystal size broadening (*ptec*), and anisotropic microstrain broadening (S_{hkl}) also were included. The d-spacing range for all refinements was 5.0–1.3 Å (2θ range: 9° - 37.5°). After the above parameters had converged, atomic positions, isotropic temperature factors (U_{iso}), and iron occupancies in hematite were allowed to refine. Representative refinements of our reaction products are shown in the Supporting Information (Tables S3, S4, and Fig. S3).

2.4. Characterization of crystal morphology

We observed end-product crystal morphologies and particle sizes from our batch experiments using field emission scanning electron microscopy (FE-SEM) and transmission electron microscopy (TEM). For SEM analyses, sample powders were ultrasonically dispersed in ethanol, then transferred to and dried on double-sided sticky carbon tape, and finally coated with 5 nm of iridium (Ir) to prevent sample charging. The SEM images were obtained using a Scios 2 FE-SEM (Materials Characterization Laboratory, Pennsylvania State University) with an accelerating voltage of 5 keV and beam current of 50 pA. For TEM analyses, samples were first dispersed in ethanol by ultrasonication and then air-dried on a holey carbon film on Cu grids. TEM images were acquired using a FEI Talos F200X (S)TEM (Materials Characterization Laboratory, Pennsylvania State University) at an acceleration voltage of 200 kV.

3. Results and discussion

3.1. Transformation of ferrihydrite to hematite and goethite

The starting Fe (hydr)oxide gels were identified as 2-line ferrihydrite using X-ray diffraction based on two broad peaks at 2.50 and 1.45 Å, consistent with other studies (Schwertmann and Cornell, 1992; Schwertmann et al., 2004; Michel et al., 2007). No significant differences in the starting two-line ferrihydrite samples were discernible with wide-angle synchrotron XRD, regardless of initial pH (Fig. 2A). Water introduced broad but low background humps at ~3.18 and 2.11 Å (1/d = 0.31 and 0.47 $Å^{-1}$), and the quartz capillary contributed an additional minor background hump at ~4.17 Å (1/d = 0.24 $Å^{-1}$) (Fig. 2B). As more KOH was added to the iron nitrate solution to increase pH, more ferrihydrite precipitated (Schwertmann and Cornell, 1992). Thus, the diffraction pattern for the ferrihydrite gel at pH 12 had a greater peak-to-background intensity ratio than was the case at pH 2. The ferrihydrite gel at pH 13 spontaneously transformed to goethite at room temperature.

Hematite and/or goethite were the only transformation products from ferrihydrite in our batch and capillary experiments. No

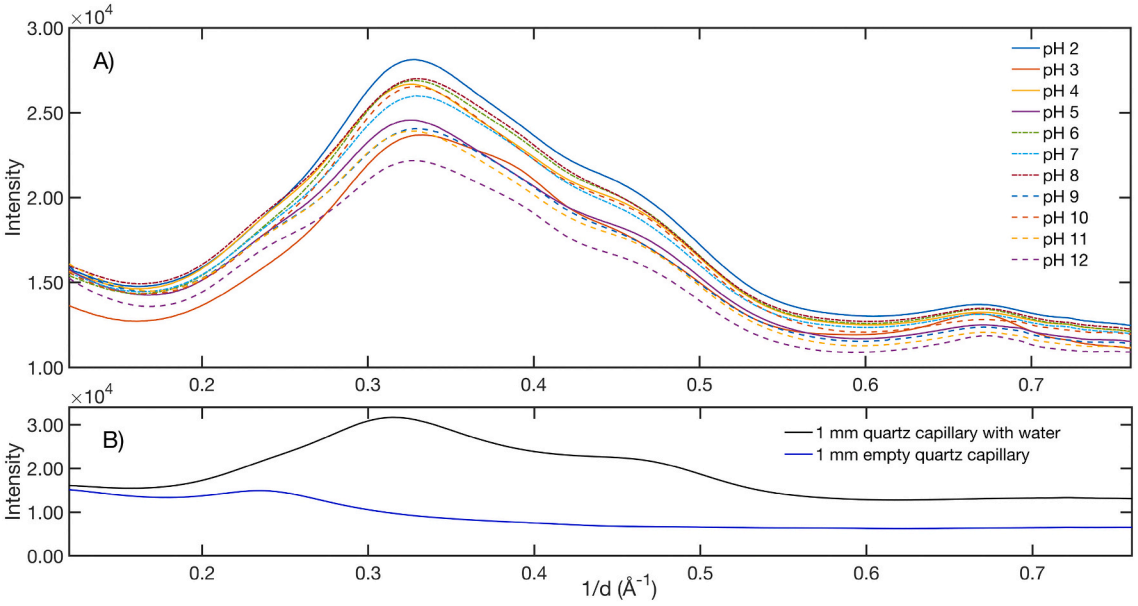

Fig. 2. (A) Synchrotron XRD patterns of fresh two-line ferrihydrite (Fh) at initial pH 2–12 in quartz capillaries at room temperature. Two-line ferrihydrite has two characteristic broad peaks at 2.50 and 1.45 Å (1/d = 0.4 and 0.69 $Å^{-1}$). (B) Synchrotron XRD patterns of an empty quartz capillary and of a quartz capillary with water.

intermediate phases, such as lepidocrocite (γ-FeOOH) (Boland et al., 2014), six-line ferrihydrite ($5Fe_2O_3 \bullet 9H_2O$) (Jansen et al., 2002; Kukkadapu et al., 2003; Burleson and Penn, 2006), or maghemite (γ-Fe_2O_3) (Liu et al., 2008) were observed, as reported by other studies on the ferrihydrite to hematite/goethite transformation. The appearance of these intermediate phases is caused by foreign ions, such as Fe^{2+}, hydrogen carbonate (HCO_3^-), phosphate (PO_4^{3-}), *etc.* Hematite and/or goethite are the primary alteration products of pure ferrihydrite at any pH or temperature, in either anoxic or oxic conditions.

In our TRXRD experiments at 130 °C, we observed that only hematite precipitated when the initial pH ranged from 2 to 5 (Fig. 3). The relative abundance of hematite within the X-ray beam footprint can be quantified through refined scale factors, which are fitting parameters that scale the calculated intensities to the observed intensities. We normalized the scale factor for each pattern to the scale factor refined for the final pattern of each run to determine the relative change in mass with time. As seen in Fig. 4, hematite continuously precipitated from ferrihydrite until reaching a plateau at 2000 s, at which point ferrihydrite was exhausted.

In contrast, between pH 6 and 12 at 130 °C, *in situ* XRD revealed that both hematite and goethite crystallized from ferrihydrite (Fig. 5). In Fig. 6, the refined scale factors for hematite and goethite are plotted as a function of time for starting pH values of 6 and 9, indicating the relative amounts of hematite and goethite during crystallization. Over this pH range, the precipitation of hematite and goethite occurred in four stages: 1) hematite and goethite diffraction peaks emerged almost simultaneously, indicating near-concurrent nucleation of the two phases from the ferrihydrite gel; 2) the growth of hematite outpaced the formation of goethite until a steady-state ratio was achieved; 3) hematite and goethite continued to co-precipitate at that steady-state proportion so long as ferrihydrite remained; 4) as the ferrihydrite depleted, the growth of hematite and goethite slowed and then terminated, with no further increase in mass abundance. Although roughly equal amounts of goethite and hematite formed initially, the more rapid rate of hematite production relative to goethite likely resulted from a rapid pH decrease from the initial values. Nevertheless, the final ratios of hematite-to-goethite,

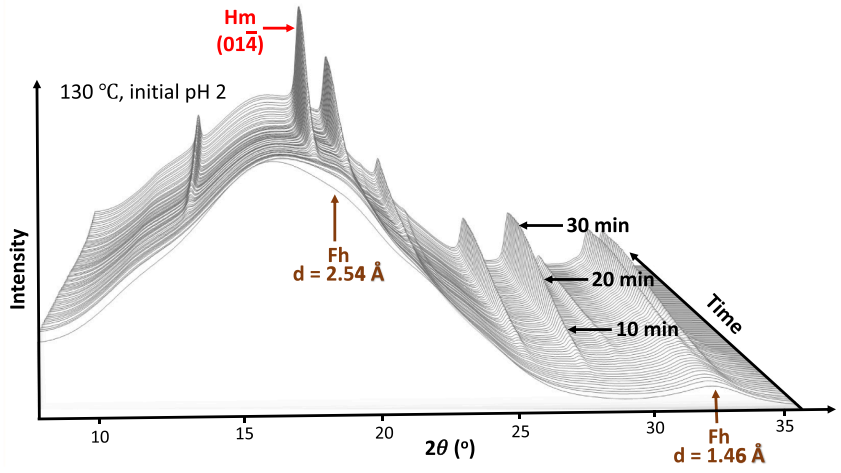

Fig. 3. Stacked TRXRD patterns showing the crystallization of hematite from two-line ferrihydrite at 130 °C, initial pH 2.

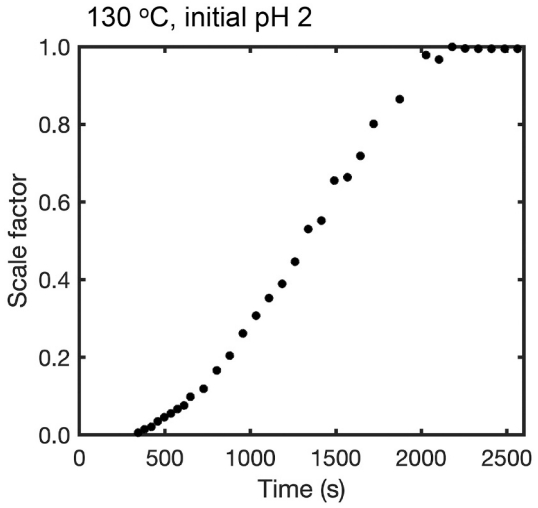

Fig. 4. Changes in refined scale factors (normalized to the final refined scale factor) for hematite with time at 130 °C, initial pH 2.

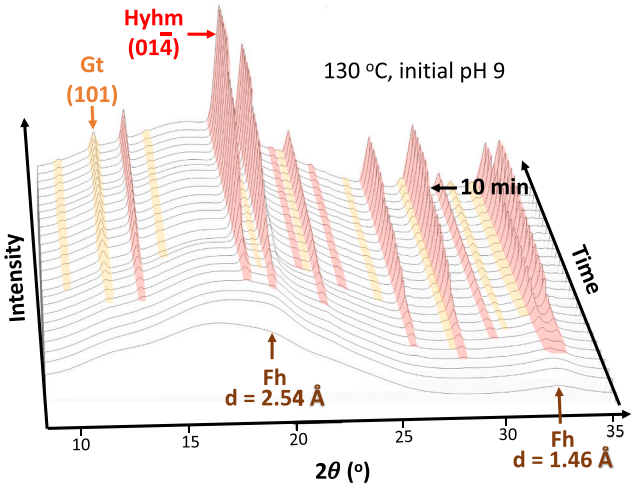

Fig. 5. Stacked TRXRD patterns showing the crystallization of hematite (red peaks) and goethite (yellow peaks) from 2-line ferrihydrite at 130 °C, initial pH 9. (For interpretation of the references to color in this figure legend, the reader is referred to the web version of this article.)

and the rates of precipitation, showed a strong dependence on the initial pH. (A full kinetic analysis of Fe (oxyhydr)oxide crystallization will be treated in a separate paper).

It was notable that the hematite-goethite ratio remained constant during the final crystal growth stage; this behavior was reproduced for other combinations of temperature and pH in our experiments (Chen et al., 2021). Likewise, when ferrihydrite was sufficiently abundant, a constant hematite-goethite ratio also was observed for low- to room-temperature systems (4 to 25 °C) in other studies (Schwertmann and Murad, 1983; Schwertmann et al., 2004). Even when unreacted ferrihydrite could still be detected, Schwertmann et al. (2004) observed that the hematite-goethite ratio scarcely changed after 441 days over a wide pH range. We also sampled our room temperature (25 °C) products after 40, 300, 1240, and 1517 days. Within error, the changes in the hematite-goethite ratio were not measurable after 300 days. However, the dried products were poorly crystalline, and significant quantities of ferrihydrite persisted at 300 days. The broad diffraction peaks from two-line ferrihydrite generated a background that was hard to distinguish from the poorly crystalline hematite and goethite in our room temperature samples; thus, quantifying hematite and goethite in these runs was limited by errors up to 10 wt%, even using synchrotron XRD.

The co-precipitation of hematite and goethite raised the possibility that the two phases were intergrown. Using HRTEM, Chen et al. (2021) observed alternating bands of hematite and goethite in natural botryoidal samples that revealed lattice coherence at the interface. However, examination of the products in the present experiments by scanning and transmission electron microscopy did not support this inference. SEM images (Fig. 7A) revealed that when only hematite precipitated (initial pH 2 to 5), the crystals formed as rhombic platelets with an average diameter of 100 ± 20 nm. When the products contained a mixture of hematite and goethite, nanoparticles were aggregated such that hematite and goethite could not be morphologically distinguished within the resolution of the SEM (Fig. 7B). Nevertheless, TEM images of these mixtures (Fig. 7C) allowed for the unambiguous discrimination of hematite and goethite nanocrystals. Goethite appeared as acicular crystals with lengths of 200 ± 50 nm and widths of 15 ± 5 nm. Hematite, on the other hand, occurred as equant crystals that were predominantly diamond-shaped with an average diameter of 60 ± 10 nm. Fast Fourier transforms (FFT) of high-resolution TEM images confirmed these identifications. Thus, even though goethite and hematite both are hexagonally closest-packed structures, TEM observations revealed that hematite and goethite precipitated as separate nanoparticles, not as layered intergrowths.

Moreover, we observed no evidence for the transformation of goethite to hematite within 48 h at 70–170 °C or even within 1517 days at 25 °C. The dehydration of goethite is extremely slow at temperatures lower than 150 °C because the activation energy for the transition of goethite to hematite is fairly high, ranging from 107 to 170 kJ/mol (Goss, 1987; Walter et al., 2001). Thermogravimetric experiments of these authors suggest that only the surface-sorbed water in goethite can be removed at temperatures below 150 °C. Goss (1987) argues that the transformation of goethite to hematite by dry heating starts at ~200 °C, and the complete transformation of goethite to hematite requires >4 days at 120 °C. Therefore, the secondary transformation of goethite to hematite observed in Vu et al. (2010) can be attributed to their experimentally high temperatures of 180–240 °C and high starting pH of 13.2.

3.2. *Hematite-goethite ratios at moderately high temperature (70–170 °C) and initial pH from 2 to 11*

To capture the relative contributions of pH and temperature to the transformation of ferrihydrite, we fit our non-RT data to a smooth surface using a local weighted regression (Fig. 8A) and projected the surface from 3D to 2D in Fig. 8B using MATLAB R2020b (Martinez et al., 2017). These experiments further confirmed that higher temperatures induced higher hematite-goethite ratios at all initial pH concentrations, suggesting that thermodynamic forces outweigh kinetic factors at higher temperatures. It should be noted, however, that reaction progress was not identical for all conditions studied. When the heating temperature was 90 °C or higher, ferrihydrite had completely reacted in all runs. However, when the temperature was lower than 90 °C, the transformation was incomplete after 48 h for some combinations of pH and temperature. Residual ferrihydrite was observed for the initial pH 2–8 at 70 °C and pH 6–8 at 80 °C, suggesting slow reaction kinetics in neutral conditions.

As seen in Fig. 8, at initial pH 2–5, hematite dominated relative to goethite when the temperature exceeded 80 °C, with goethite present at <20 wt% of the final product. However, the hematite-goethite ratio dropped sharply at 70 °C (Fig. 8) and 25 °C at pH 2 (Fig. 9), such that goethite accounted for 98 wt% of the precipitate at these lower temperatures. Previous studies support our observations that only hematite forms at temperatures higher than 90 °C when ferrihydrite or akageneite is the reaction precursor at initial pH ≤ 2 (Johnston and Lewis, 1983; Das et al., 2011; Peterson et al., 2016). Conversely, over 90 wt% of the ferrihydrite reaction product is goethite at pH 2 when the temperature is

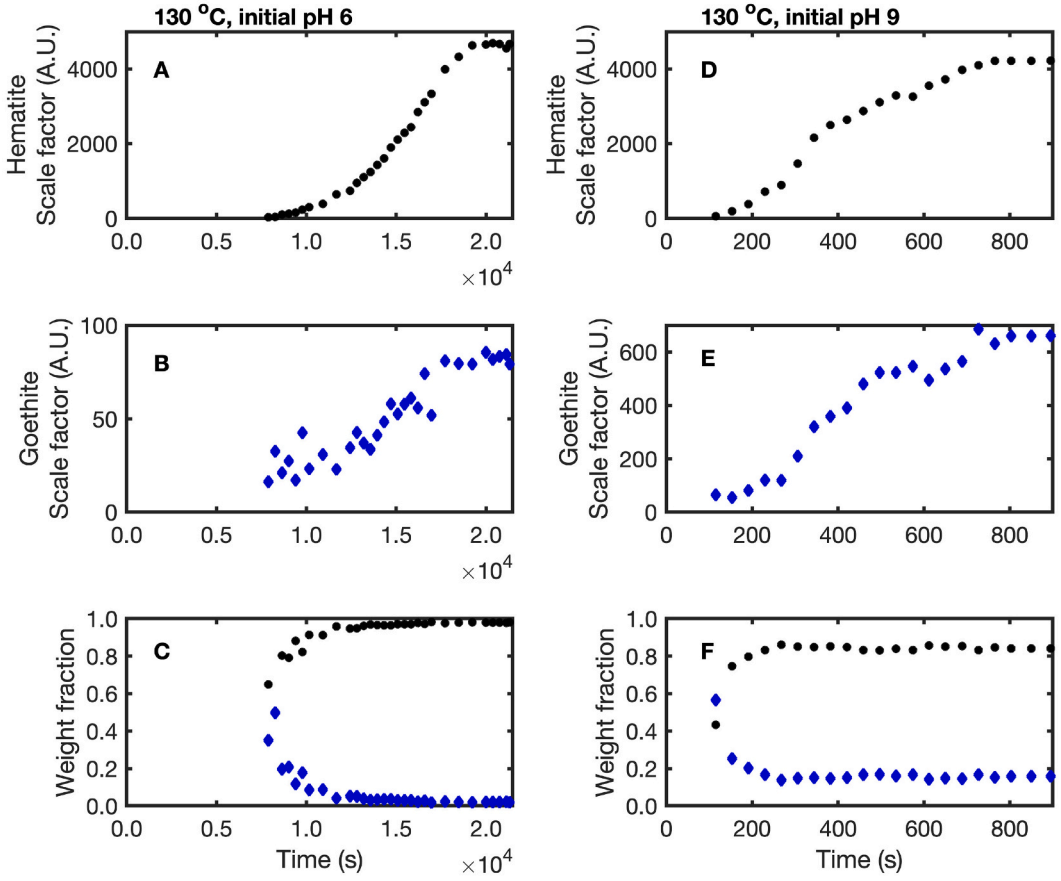

Fig. 6. The growth of hematite and goethite with time from representative TRXRD experiments. Changes in refined scale factors and weight fractions for hematite (black dots) and goethite (blue squares) with time at 130 °C and initial pH of 6 (left column) and 9 (right column). Weight fractions of hematite and goethite were constrained to sum to 1.0. (For interpretation of the references to color in this figure legend, the reader is referred to the web version of this article.)

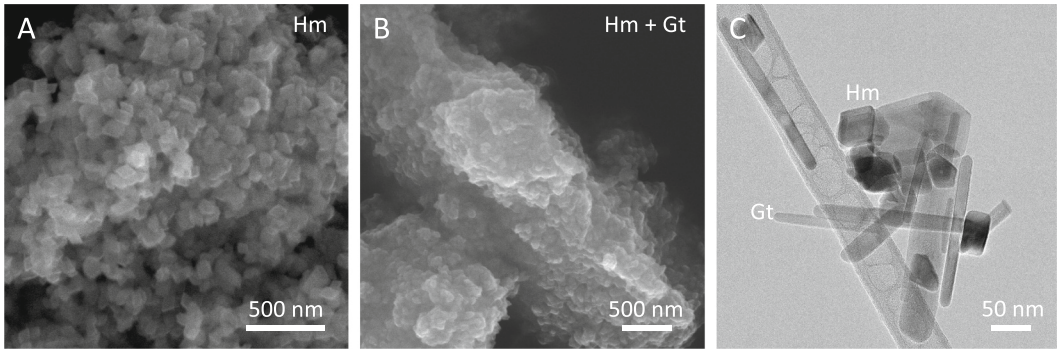

Fig. 7. SEM images of pure hematite (A) obtained by heating the ferrihydrite gel (initial pH at 4) at 110 °C for 48 h. A mixture (B) of 60 wt% hematite (Hm) and 40 wt% goethite (Gt) synthesized from initial pH 6 and heating at 110 °C for 48 h. (C) Bright-field TEM image of the sample in (B). Hematite appeared as hexagonal plates with an average diameter of 60 ± 10 nm, whereas goethite occurred as acicular crystals with lengths of 200 ± 50 nm and widths of 15 ± 5 nm.

lower than 50 °C (Schwertmann and Murad, 1983; Schwertmann et al., 2004; Das et al., 2011). Although hematite is thermodynamically favored even at low pH (Grønvold and Samuelsen, 1975; Laberty and Navrotsky, 1998), the activation barrier to hematite crystallization is relatively high at pH 2 (Vu et al., 2008; Francisco et al., 2016). Thus, kinetic barriers override thermodynamics below 70 °C, leading to a dramatic drop in the hematite-goethite ratio.

At higher initial pH values, the greater hydroxyl concentrations promoted goethite formation, and the hematite-goethite ratios decreased to a minimum at an initial pH ~ 7 (Figs. 8, 9). When the starting pH was in the range of 9 to 10, hematite again dominated even at low temperatures, despite the higher concentration of OH^-. We argue that the increase in hematite-goethite ratios at initial pH 9–10 may be explained by the formation of superhydrous hematite rather than stoichiometric hematite (Wolska, 1981; Gualtieri and Venturelli, 1999; Chen, 2021; Chen et al., 2021). Our Rietveld refinements revealed that a hydrous hematite, named hydrohematite (Wolska, 1981; Gualtieri and Venturelli, 1999; Peterson et al., 2015; Chen et al., 2021), forms in alkaline conditions in both *in-situ* and *ex-situ* experiments (Table S5 and S6). For example, the refined Fe occupancy of hematite formed at a starting pH of 2 was 1.00(1), whereas at an initial pH of 10, Fe_{occ} was 0.91(2) in our batch experiments (Table S5). The differences in the X-ray

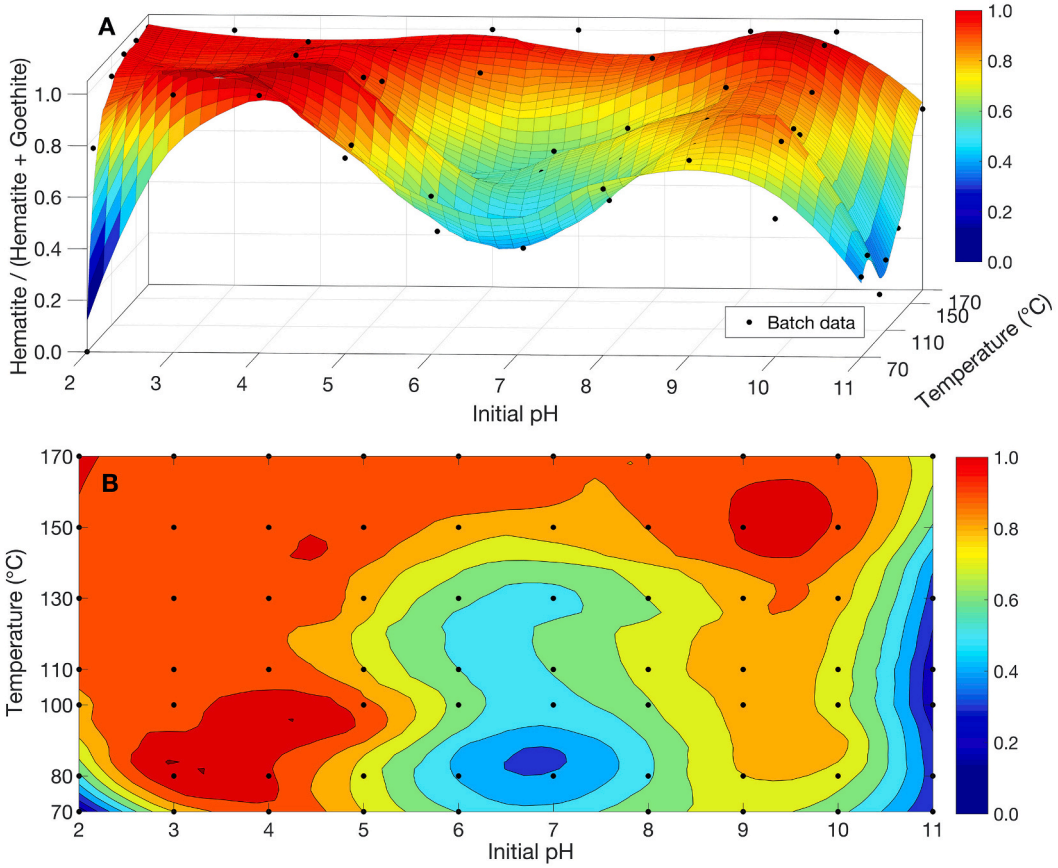

Fig. 8. Hematite-goethite ratios as a function of initial pH and temperature (T) as fit using a 3D surface (A) and as projected in 2D (B). Black dots represent batch experimental data for reactions starting with a 0.2 *M* ferrihydrite gel. Final goodness-of-fit (GOF) parameters of the surface fitting to our experimental data were: R^2 = 0.9426, SSE = 0.2089, and RMSE = 0.0614.

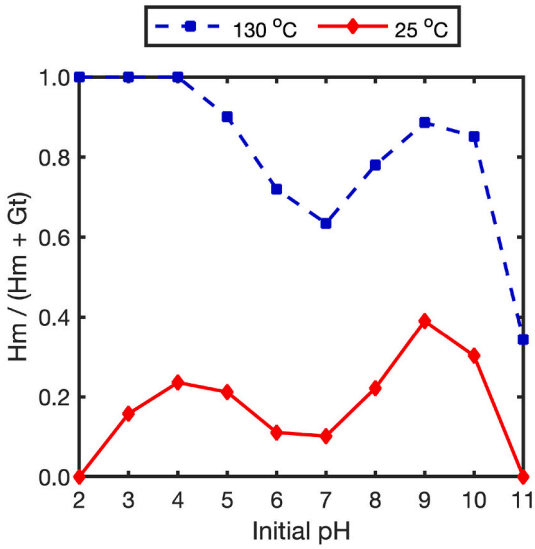

Fig. 9. Hematite (Hm)-to-goethite (Gt) ratios as a function of initial pH at 130 °C and 25 °C. Data represent batch experiments with 0.2 *M* ferrihydrite gels after reaction for 1517 days (25 °C) and 48 h (130 °C). Higher temperatures strongly favored hematite formation at all initial pH concentrations.

diffraction patterns produced by hydrohematite and stoichiometric hematite are demonstrated in the Supporting Information (Fig. S4). The refined Fe occupancies of our synthetic hematite varied from 0.6 to 1.0 based on reaction time, heating temperature, and pH concentration (Chen et al., 2021). A comprehensive structural analysis will be presented in a separate paper. The general formula for hydrohematite is $Fe_{2-x/3}O_{3-x}(OH)_x$ (Wolska, 1981), with iron concentrations ranging from 0.80 to 0.90 and water contents of 7.80 to 3.63 wt%, as identified in natural hydrohematite specimens (Wolska, 1981; da Cunha and da Costa, 2016; Chen et al., 2021). The Fe occupancies of hydrohematite in these studies were analyzed by XRD and electron probe microanalysis (EPMA), and hydroxyl contents were further confirmed by infrared spectroscopy (FTIR) and thermogravimetric analysis coupled with mass spectrometry (TGA-MS). Because OH^- groups are incorporated in hydrohematite, we speculate that it is energetically favored relative to stoichiometric hematite in slightly alkaline conditions, even outcompeting goethite in our experiments.

Highly alkaline conditions (initial pH $\geq$ 11) always favored goethite formation because of the excess hydroxyl concentrations in solution, consistent with previous studies (Lewis and Schwertmann, 1980; Johnston and Lewis, 1983; Schwertmann and Murad, 1983; Schwertmann et al., 2004; Shaw et al., 2005; Vu et al., 2010; Heaney et al., 2020). At pH 13 and 90 °C, goethite was the only phase to form.

3.3. *Divergence of our results from the classical model of Schwertmann and Murad (1983)*

Schwertmann and Murad (1983) were the first to perform a comprehensive study of the ferrihydrite to hematite/goethite transformation as a function of pH. Their study targeted pH concentrations ranging from 2 to 11, and they were all conducted at room temperature (24 °C) (Fig. 10A). After ferrihydrite had aged for 441 days in their

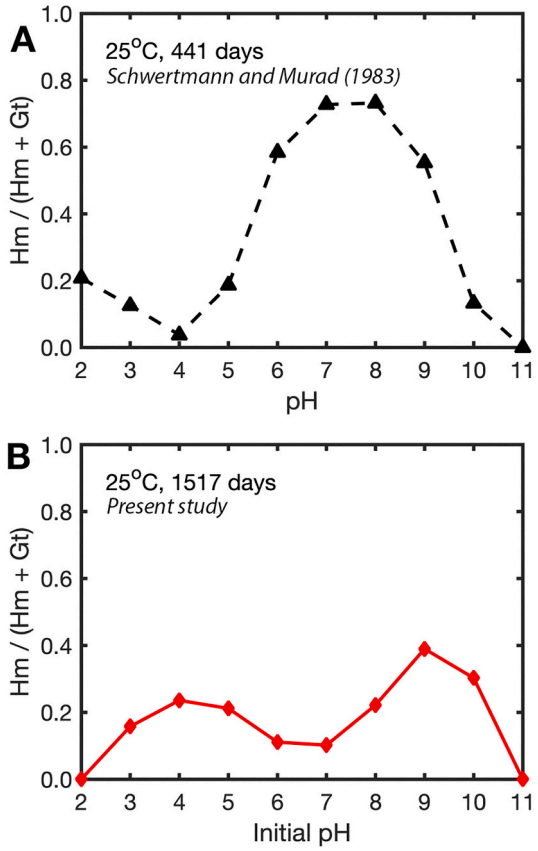

Fig. 10. Hematite (Hm) to goethite (Gt) ratios for ferrihydrite aged at 25 °C for 441 days from Schwertmann and Murad (1983) (A) and for 1517 days in the present study (B).

experiments, these authors observed that hematite formation was maximized at pH 7–8, whereas goethite formation was favored at pH 4 and 12. These results contrast with the behaviors we observed for our room-temperature experiments (25 °C, Fig. 10B). After aging ferrihydrite for 1517 days at 25 °C in our batch experiments, only goethite formed at pH 2 and pH 11, whereas hematite was favored in mildly acidic (pH 3–5) and mildly alkaline conditions (pH 9–10).

What is the cause of these discrepancies? The experimental protocols in Schwertmann and Murad (1983) and Schwertmann et al. (2004) were different from ours in the following respects: 1) these authors prepared ferrihydrite by titrating a 0.1 *M* iron nitrate ($Fe(NO_3)_3$) solution with ammonium hydroxide (NH_4OH) to pH 7.5 to 8, and they then adjusted the washed ferrihydrite suspensions to pH 2 to 12 by adding HNO_3 or NaOH; 2) they readjusted pH every several months, whereas our experiments were unbuffered. The starting $Fe(NO_3)_3$ solution was very acidic, with pH <1.0. Because NH_4OH ($pK_b = 4.75$) is a weaker base than the titrant we used (KOH with $pK_b = 0.5$), achieving the initial pH of 7.5–8.0 would have required significant dilution of the ferrihydrite mixture. Moreover, the authors do not specify the volume and molarity of the HNO_3 and NaOH titrants they used for subsequent pH adjustments. Out of concern that the repeated dilution and the pH fluctuations entailed in this protocol could introduce disaggregation/aggregation cycles of the ferrihydrite nanoparticles (Baalousha, 2009), we set pH at the beginning of our experiments and did not alter the ferrihydrite gels thereafter. Presumably, the differences in our experimental approaches explain the different behaviors.

3.4. pH changes during the transformation of iron oxides

As hematite and goethite precipitated from ferrihydrite, the pH changed, consistent with observations in other studies (Bao and Koch, 1999; Brinza et al., 2015; Scheck et al., 2016). The measured pH values of each solution after the reactions had progressed for 48 h in our batch experiments are listed in Table 1 and in the Supporting Information (Table S2). When the initial pH ranged from 2 to 5, the pH dropped to between 1.0 and 2.5 as the ferrihydrite completely reacted, consistent with previous studies (Bao and Koch, 1999; Scheck et al., 2016). When the initial pH was 6–7, the final pH exhibited a much broader variation, from 2.2 to 6.5, dependent predominantly on the degree of reaction at different temperatures. For example, a complete transformation of ferrihydrite to hematite and goethite with an initial pH of 6–7 resulted in a final pH of 2.2–2.5 at 110–170 °C. However, when ferrihydrite was heated at 80 °C for 48 h, the reaction was not complete and pH dropped from 6.0 to 4.4. In contrast to these decreases in pH, when the initial pH ranged from 9 to 11, the pH values increased by 1 to 2 units by the time the transformation was completed.

$$Fe(OH)^{2+} + H_2O \longrightarrow \alpha - FeOOH\ (Goethite) + 2H^+ \quad (1)$$

$$2Fe(OH)^{2+} + H_2O \longrightarrow \alpha - Fe_2O_3\ (Hematite) + 4H^+ \quad (2)$$

$$Fe(OH)_2^{+} \longrightarrow \alpha - FeOOH\ (Goethite) + H^+ \quad (3)$$

$$2Fe(OH)_2^{+} \longrightarrow \alpha - Fe_2O_3\ (Hematite) + H_2O + 2H^+ \quad (4)$$

$$Fe(OH)_4^{-} \longrightarrow \alpha - FeOOH\ (Goethite) + H_2O + OH^- \quad (5)$$

$$2Fe(OH)_4^{-} \longrightarrow \alpha - Fe_2O_3\ (Hematite) + H_2O + 2OH^- \quad (6)$$

The variations in final pH can be explained by the reactions of Fe(III) ions (Eqs. (1)–(6)) at different pH conditions. These reactions offer insights into the concentrations of different Fe(III) species at equilibrium (Fig. 11, Supplementary Information II), as calculated using thermodynamic data with the Visual MINTEQ v3.0 database (Gustafsson, 2014), which incorporates the NIST Critical Stability constants database (Smith, 2010). In acidic solutions (pH $\leq$ 4), the predominant Fe(III) species is $Fe(OH)^{2+}$. The transformation of $Fe(OH)^{2+}$ to either hematite or goethite (Eq. (2)) results in a release of protons. Consequently, pH decreased when the initial pH in our experiments was below 4. Similarly, the transformation of $Fe(OH)_4^-$ to hematite and goethite in alkaline solutions (pH $\geq$ 9) yields an increase in OH^-, leading to the increase in pH that we observed (Eqs. (5)–(6)).

However, the pH changes at circumneutral to neutral conditions are more complex, and the reaction sequences are less clearly understood. The concentrations of different Fe(III) ions in equilibrium, such as $Fe(OH)^{2+}$, $Fe(OH)_2^+$, or $Fe(OH)_4^-$, depend strongly on temperature. For example, at pH 8, $Fe(OH)_2^+$ dominates at 25 °C, whereas $Fe(OH)_4^-$ dominates at temperatures above 70 °C (Misawa, 1973). Because different Fe(III) ion reactions yield different concentrations of protons or hydroxyls, the final pH for circumneutral solutions (pH 6–8) was influenced by the dominant Fe(III) species and the final hematite-goethite ratios.

3.5. Water activity

The transformation of ferrihydrite to hematite and goethite in soils typically is mediated by water (Bowles, 1992; Cornell and Schwertmann, 2003; Schwertmann et al., 2004). The hematite-goethite ratio varies with water activity, and the ratio has been used to reconstruct paleorainfall records across wide climate regimes in aerobic or anaerobic conditions (Kämpf and Schwertmann, 1983; Camargo et al., 2013; Hyland et al., 2015; Lagroix et al., 2016; Long et al., 2016; Silva et al., 2020; Lepre and Olsen, 2021). As suggested by these studies, more humid environments favor goethite, so that the hematite-goethite ratios decrease with increasing moisture (rainfall minus evapotranspiration).

Although our study did not systematically investigate the effects of water activity on hematite-goethite ratios, we did compare iron

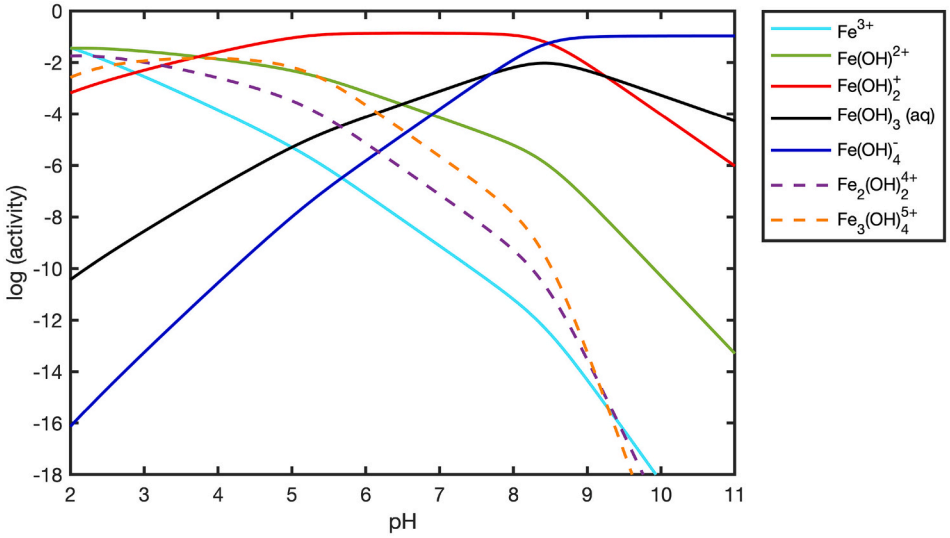

Fig. 11. Fe(III) ion species as a function of pH at 25 °C.

(oxyhydr)oxide precipitation from 0.2 *M* and 1.0 *M* ferrihydrite gels at 130 °C (Fig. 12). The general trends in hematite-goethite ratios were similar across initial pH for the two ferrihydrite concentrations, but above pH 4, more goethite precipitated relative to hematite when the concentration of ferrihydrite was lower, supporting previous studies that higher water activities enhance goethite formation. In addition to the role that water is playing in the formation of the more hydrous goethite, higher ferrihydrite concentrations facilitate the hydrolysis processes by which nanoparticles aggregate, thus enhancing hematite formation (Scheck et al., 2016).

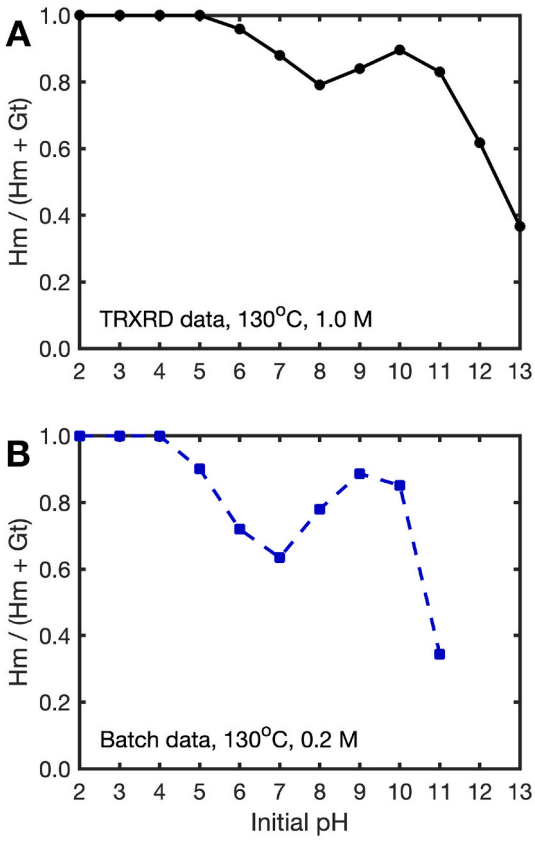

Fig. 12. Dependence of hematite-goethite ratios on pH for 1.0 *M* (A) and 0.2 *M* (B) ferrihydrite gels. Higher water activity favored goethite precipitation for pH ≥ 5.

4. Conclusion

The relative abundances of hematite and goethite in soils and sedimentary rocks have been used to interpret monsoonal and El Niño cyclicity over 1 to >100 ka timescales (Ji et al., 2004; Zhang et al., 2007; Clift et al., 2019), to estimate mean annual paleoprecipitation (Hyland et al., 2015; Long et al., 2016), and to explain sedimentary paleomagnetism (Liu et al., 2007, 2008). In addition, hematite-goethite ratios strongly influence soil color (particularly of terra rossa soils) and thus are a primary focus of visible light remote sensing on Earth and other planets (Barrón and Torrent, 2002; Jiang et al., 2022).

Prior to the present study, the seminal work by Schwertmann and Murad (1983) has dominated interpretations about the relationship between hematite-goethite ratios and solution pH. As described above, however, that work attempted to maintain constant pH during the ferrihydrite to hematite-goethite reaction, as would be appropriate to model systems with a high pH buffering capacity. The authors state, however, that "pH was readjusted at first at weekly intervals, later once every several months". In light of our observations that titration of ferrihydrite gels is followed by a return to the previous pH within a matter of days, we infer that the ferrihydrite samples in that study followed a saw-tooth variation in pH, with long periods at the steady-state pH followed by brief, sharp upticks after the monthly adjustments.

The present work is more directly applicable to environments that lack the pH buffering capacity to maintain an initial circumneutral pH – for example, soils exposed to acid-waste drainage and soils with low concentrations of organic matter and/or minerals with exchangeable cations (Curtin and Trolove, 2013). Our study reveals that: 1) Even when systems are unbuffered, the crystallization pathway during the transformation of ferrihydrite will vary significantly in response to the initial pH; 2) When ferrihydrite is unbuffered, hematite precipitation is favored at pH 3–6 and pH 9–10 relative to neutral pH; 3) The nucleation of hematite and goethite from ferrihydrite can occur concurrently, explaining why hematite and goethite typically co-occur in soils and sedimentary rocks; 4) Fe-deficient, superhydrous hematite can form in slightly alkaline conditions over a broad temperature range from at least 25 to 180 °C. The substitution of H^+ for Fe^{3+} will alter the color and magnetic properties of the hematitic phase (Pailhé et al., 2008; Liu et al., 2010).

Evaluating the usefulness of hematite-goethite ratios as a paleoproxy

likely requires a deeper understanding of the mechanism by which this transformation occurs. The changes in solution pH that we measured challenge the conventional mechanism invoked for this reaction – that hematite forms through dehydration and internal structural rearrangement of ferrihydrite, whereas goethite forms through dissolution and reprecipitation (Schwertmann and Murad, 1983; Cornell and Schwertmann, 2003). Even the formation of hematite appears to require the participation of dissolved Fe species, but the interplay between these species and the poorly crystalline ferrihydrite remains ill-constrained. To fully understand the formation of iron oxides in natural environments, more work in controlled systems is required, including investigations of properly buffered transformations of ferrihydrite.

Declaration of Competing Interest

None.

Acknowledgments

Funding for this research was provided by the National Science Foundation Grant EAR-1552211 and EAR-1925903, the Pennsylvania State University Biogeochemistry dual-title Ph.D. program, and the Hiroshi and Koya Ohmoto Graduate Fellowship from the Pennsylvania State University Geosciences Department. Synchrotron XRD was performed at the GSECARS (University of Chicago) Beamline 13-BM-C at the APS. GSECARS is supported by NSF EAR-1634415 and DOE GeoSciences DE-FG02-94ER14466. APS is operated under DOE Contract No. DE-AC02-06CH11357. We acknowledge Devon Chenot for his help with pH measurements. We thank four anonymous reviewers for their helpful suggestions and comments.

Appendix A. Supplementary data

Supplementary data to this article can be found online at https://doi.org/10.1016/j.chemgeo.2022.120995.

References

Baalousha, M., 2009. Aggregation and disaggregation of iron oxide nanoparticles: Influence of particle concentration, pH and natural organic matter. Sci. Total Environ. 407, 2093–2101. https://doi.org/10.1016/j.scitotenv.2008.11.022.

Bao, H., Koch, P.L., 1999. Oxygen isotope fractionation in ferric oxide-water systems: low temperature synthesis. Geochim. Cosmochim. Acta 63, 599–613. https://doi.org/10.1016/S0016-7037(99)00005-8.

Barrón, V., Torrent, J., 2002. Diffuse Reflectance Spectroscopy of Iron Oxides. Encycl. Surf. Colloid Sci. 1, 1438–1446. https://www.researchgate.net/publication/264869284.

Blake, R.L., HessevicK, R.E., Zoltai, T., Finger, L.W., 1966. Refinement of the Hematite Structure. Am. Mineral. 51, 123–129.

Boland, D.D., Collins, R.N., Miller, C.J., Glover, C.J., Waite, T.D., 2014. Effect of solution and solid-phase conditions on the Fe(II)-accelerated transformation of ferrihydrite to lepidocrocite and goethite. Environ. Sci. Technol. 48, 5477–5485. https://doi.org/10.1021/es4043275.

Bowles, J.F.W., 1992. U. Schwertmann and R. M. Cornell Iron Oxides in the Laboratory. Weinheim, New York, Basel and Cambridge (VCH), 1991. xiv + 137 pp. Price £45.00. Mineral. Mag. 56, 281–282. https://doi.org/10.1180/minmag.1992.056.383.20.

Brinza, L., Vu, H.P., Shaw, S., Mosselmans, J.F.W., Benning, L.G., 2015. Effect of Mo and v on the hydrothermal crystallization of hematite from ferrihydrite: an in situ energy dispersive X-ray diffraction and X-ray absorption spectroscopy study. Cryst. Growth Des. 15, 4768–4780. https://doi.org/10.1021/acs.cgd.5b00173.

Burleson, D.J., Penn, R.L., 2006. Two-step growth of goethite from ferrihydrite. Langmuir 22, 402–409. https://doi.org/10.1021/la051883g.

Camargo, L.A., Marques, J., Pereira, G.T., 2013. Mineralogia da fração argila de um Argissolo em Curvaturas do relevo. II - correlação especial com atributos físicos. Rev. Bras. Cienc. do Solo 37, 307–316. https://doi.org/10.1590/S0100-06832013000200002.

Carlson, L., Schwertmann, U., 1981. Natural ferrihydrites in surface deposits from Finland and their association with silica. Geochim. Cosmochim. Acta 45. https://doi.org/10.1016/0016-7037(81)90250-7.

Chen, S.A., 2021. The formation of iron (hydr)oxides in surface environments: a crystallographic and kinetic study. Pennsylvania State University. https://etda.libraries.psu.edu/catalog/19553szc81.

Chen, S.A., Heaney, P.J., Post, J.E., Fischer, T.B., Eng, P.J., Stubbs, J.E., 2021. Superhydrous hematite and goethite: a potential water reservoir in the red dust of Mars? Geology 49 (11), 1343–1347. https://doi.org/10.1130/G48929.1.

Childs, C.W., 1992. Ferrihydrite: a review of structure, properties and occurrence in relation to soils. Z. Pflanzenernähr. Bodenkd. 155, 441–448. https://doi.org/10.1002/jpln.19921550515.

Christensen, P.R., Morris, R.V., Lane, M.D., Bandfield, J.L., Malin, M.C., 2001. Global mapping of Martian hematite mineral deposits: Remnants of water-driven processes on early Mars. J. Geophys. Res. E Planets 106, 23873–23885. https://doi.org/10.1029/2000JE001415.

Clift, P.D., Kulhanek, D.K., Zhou, P., Bowen, M.G., Vincent, S.M., Lyle, M., Hahn, A., 2019. Chemical weathering and erosion responses to changing monsoon climate in the late Miocene of Southwest Asia. Geol. Mag. https://doi.org/10.1017/S0016756819000608.

Colombo, C., Palumbo, G., He, J.Z., Pinton, R., Cesco, S., 2014. Review on iron availability in soil: Interaction of Fe minerals, plants, and microbes. J. Soils Sediments 14, 538–548. https://doi.org/10.1007/s11368-013-0814-z.

Cornell, R.M., Schwertmann, U., 2003. The Iron Oxides. Structures, Properties, Reactions, Occurences and Uses.

Curtin, D., Trolove, S., 2013. Predicting pH buffering capacity of New Zealand soils from organic matter content and mineral characteristics. Soil Res. 51, 494–502. https://doi.org/10.1071/SR13137.

da Cunha, C.C.R.F., da Costa, G.M., 2016. Water determination in iron oxyhydroxides and iron ores by Karl Fischer titration. Phys. Chem. Miner. 43, 739–748. https://doi.org/10.1007/s00269-016-0830-9.

Das, S., Hendry, M.J., Essilfie-Dughan, J., 2011. Transformation of two-line ferrihydrite to goethite and hematite as a function of pH and temperature. Environ. Sci. Technol. 45, 268–275. https://doi.org/10.1021/es101903y.

Ferris, F.G., 2005. Biogeochemical properties of bacteriogenic iron oxides. Geomicrobiol J. 22, 79–85. https://doi.org/10.1080/01490450590945861.

Fraeman, A.A., Arvidson, R.E., Catalano, J.G., Grotzinger, J.P., Morris, R.V., Murchie, S. L., Stack, K.M., Humm, D.C., McGovern, J.A., Seelos, F.P., Seelos, K.D., Viviano, C.E., 2013. A hematite-bearing layer in gale crater, mars: Mapping and implications for past aqueous conditions. Geology 41, 1103–1106. https://doi.org/10.1130/G34613.1.

Franciscco, P.C.M., Sato, T., Otake, T., Kasama, T., 2016. Kinetics of Fe3+ mineral crystallization from ferrihydrite in the presence of Si at alkaline conditions and implications for nuclear waste disposal. Am. Mineral. 101, 2057–2069. https://doi.org/10.2138/am-2016-5589.

Goss, C.J., 1987. The Kinetics and Reaction Mechanism of the Goethite to Hematite Transformation. Mineral. Mag. 51, 437–451. https://doi.org/10.1180/minmag.1987.051.361.11.

Grønvold, F., Samuelsen, E.J., 1975. Heat capacity and thermodynamic properties of α-Fe2O3 in the region 300-1050 K. antiferromagnetic transition. J. Phys. Chem. Solids 36, 249–256. https://doi.org/10.1016/0022-3697(75)90017-7.

Gualtieri, A.F., Venturelli, P., 1999. In situ study of the goethite-hematite phase transformation by real time synchrotron powder diffraction. Am. Mineral. 84, 895–904. https://doi.org/10.2138/am-1999-5-624.

Gustafsson, J.P., 2014. Visual MINTEQ 3. 1 user guide. KTH, Dep. L. Water Recources, Stock. Sweden, pp. 1–73.

Heaney, P.J., Oxman, M.J., Chen, S.A., 2020. A structural study of size-dependent lattice variation: in situ X-ray diffraction of the growth of goethite nanoparticles from 2-line ferrihydrite. Am. Mineral. 105, 652–663. https://doi.org/10.2138/am-2020-7217.

Hyland, E.G., Sheldon, N.D., Van der Voo, R., Badgley, C., Abrajevitch, A., 2015. A new paleoprecipitation proxy based on soil magnetic properties: Implications for expanding paleoclimate reconstructions. Bull. Geol. Soc. Am. 127, 975–981. https://doi.org/10.1130/B31207.1.

Jambor, J.L., Dutrizac, J.E., 2003. Occurrence and constitution of natural and synthetic ferrihydrite, a widespread iron oxyhydroxide. Chem. Rev. 98, 2549–2586. https://doi.org/10.1021/cr970105t.

Jansen, E., Kyek, A., Schäfer, W., Schwertmann, U., 2002. The structure of six-line ferrihydrite. Appl. Phys. A Mater. Sci. Process. 74, 1004–1006. https://doi.org/10.1007/s003390101175.

Ji, J., Chen, J., Balsam, W., Lu, H., Sun, Y., Xu, H., 2004. High resolution hematite/goethite records from Chinese loess sequences for the last glacial-interglacial cycle: Rapid climatic response of the East Asian Monsoon to the tropical Pacific. Geophys. Res. Lett. 31, 2–5. https://doi.org/10.1029/2003GL018975.

Jiang, Z., Liu, Q., Roberts, A.P., Dekkers, M.J., Barrón, V., Torrent, J., Li, S., 2022. The magnetic and color reflectance properties of hematite: from Earth to Mars. Rev. Geophys. 60 https://doi.org/10.1029/2020rg000698.

Johnston, J.H., Lewis, D.G., 1983. A detailed study of the transformation of ferrihydrite to hematite in an aqueous medium at 92°C. Geochim. Cosmochim. Acta 47, 1823–1831. https://doi.org/10.1016/0016-7037(83)90200-4.

Kämpf, N., Schwertmann, U., 1983. Goethite and hematite in a climosequence in southern Brazil and their application in classification of kaolinitic soils. Geoderma 29, 27–39. https://doi.org/10.1016/0016-7061(83)90028-9.

Kukkadapu, R.K., Zachara, J.M., Fredrickson, J.K., Smith, S.C., Dohnalkova, A.C., Russell, C.K., 2003. Transformation of 2-line ferrihydrite to 6-line ferrihydrite under oxic and anoxic conditions. Am. Mineral. 88, 1903–1914. https://doi.org/10.2138/am-2003-11-1233.

Laberty, C., Navrotsky, A., 1998. Energetics of stable and metastable low-temperature iron oxides and oxyhydroxides. Geochim. Cosmochim. Acta 62, 2905–2913. https://doi.org/10.1016/S0016-7037(98)00208-7.

Lagroix, F., Banerjee, S.K., Jackson, M.J., 2016. Geological occurrences and relevance of iron oxides. Iron Oxides From Nat. to Appl. 9–29 https://doi.org/10.1002/9783527691395.ch2.

Larson, A.C., Von Dreele, R.B., 2000. General structure analysis system (GSAS). Los Alamos National Laboratory Report LAUR 86–748.
Lepre, C.J., Olsen, P.E., 2021. Hematite reconstruction of late triassic hydroclimate over the Colorado Plateau. Proc. Natl. Acad. Sci. U. S. A. 118, 1–6. https://doi.org/10.1073/pnas.2004343118.
Lewis, D.G., Schwertmann, U., 1980. The effect of [OH] on the goethite produced from ferrihydrite under alkaline conditions. J. Colloid Interface Sci. 78, 543–553. https://doi.org/10.1016/0021-9797(80)90591-3.
Ling, F.T., Heaney, P.J., Post, J.E., Gao, X., 2015. Transformations from triclinic to hexagonal birnessite at circumneutral pH induced through pH control by common biological buffers. Chem. Geol. 416, 1–10. https://doi.org/10.1016/j.chemgeo.2015.10.007.
Liu, Q., Roberts, A.P., Torrent, J., Horng, C.S., Larrasoaña, J.C., 2007. What do the HIRM and S-ratio really measure in environmental magnetism? Geochemistry. Geophys. Geosystems 8. https://doi.org/10.1029/2007GC001717.
Liu, Q., Barrón, V., Torrent, J., Eeckhout, S.G., Deng, C., 2008. Magnetism of intermediate hydromaghemite in the transformation of 2-line ferrihydrite into hematite and its paleoenvironmental implications. J. Geophys. Res. Solid Earth 113, 1–12. https://doi.org/10.1029/2007JB005207.
Liu, Q., Barrón, V., Torrent, J., Qin, H., Yu, Y., 2010. The magnetism of micro-sized hematite explained. Phys. Earth Planet. Inter. 183, 387–397. https://doi.org/10.1016/j.pepi.2010.08.008.
Long, X., Ji, J., Barrón, V., Torrent, J., 2016. Climatic thresholds for pedogenic iron oxides under aerobic conditions: Processes and their significance in paleoclimate reconstruction. Quat. Sci. Rev. 150, 264–277. https://doi.org/10.1016/j.quascirev.2016.08.031.
Martinez, W.L., Martinez, A.R., Solka, J.L., 2017. Exploratory Data Analysis with MATLAB®. Chapman and Hall/CRC.
Michel, F.M., Ehm, L., Antao, S.M., Lee, P.L., Chupas, P.J., Liu, G., Strongin, D.R., Schoonen, M.A.A., Phillips, B.L., Parise, J.B., 2007. The structure of ferrihydrite, a nanocrystalline material. Science (80-.) 316, 1726–1729. https://doi.org/10.1126/science.1142525.
Misawa, T., 1973. The thermodynamic consideration for Fe-H2O system at 25°C. Corros. Sci. 13, 659–676. https://doi.org/10.1016/S0010-938X(73)80037-X.
Ocaña, M., Morales, M.P., Serna, C.J., 1995. The Growth Mechanism of α-Fe2O3 Ellipsoidal Particles in solution. J. Colloid Interface Sci. 171, 85–91. https://doi.org/10.1006/jcis.1995.1153.
Pailhé, N., Wattiaux, A., Gaudon, M., Demourgues, A., 2008. Impact of structural features on pigment properties of α-Fe 2O3 haematite. J. Solid State Chem. 181, 2697–2704. https://doi.org/10.1016/j.jssc.2008.06.049.
Parry, W.T., 2011. Composition, nucleation, and growth of iron oxide concretions. Sediment. Geol. 233, 53–68. https://doi.org/10.1016/j.sedgeo.2010.10.009.
Paterson, E., 1999. The Iron Oxides. Structure, Properties, Reactions, Occurrences and Uses, Clay Minerals. John Wiley & Sons. https://doi.org/10.1180/claymin.1999.034.1.20.
Peterson, K.M., Heaney, P.J., Post, J.E., Eng, P.J., 2015. A refined monoclinic structure for a variety of "hydrohematite". Am. Mineral. 100, 570–579. https://doi.org/10.2138/am-2015-4807.
Peterson, K.M., Heaney, P.J., Post, J.E., 2016. A kinetic analysis of the transformation from akaganeite to hematite: an in situ time-resolved X-ray diffraction study. Chem. Geol. 444, 27–36. https://doi.org/10.1016/j.chemgeo.2016.09.017.
Peterson, K.M., Heaney, P.J., Post, J.E., 2018. Evolution in the structure of akaganeite and hematite during hydrothermal growth: an in situ synchrotron X-ray diffraction analysis. Powder Diffract. 33, 287–297. https://doi.org/10.1017/S0885715618000623.
Prescher, C., Prakapenka, V.B., 2015. DIOPTAS: a program for reduction of two-dimensional X-ray diffraction data and data exploration. High Press. Res. 35, 223–230. https://doi.org/10.1080/08957959.2015.1059835.
Scheck, J., Wu, B., Drechsler, M., Rosenberg, R., Van Driessche, A.E.S., Stawski, T.M., Gebauer, D., 2016. The Molecular Mechanism of Iron(III) Oxide Nucleation. J. Phys. Chem. Lett. 7, 3123–3130. https://doi.org/10.1021/acs.jpclett.6b01237.
Schwertmann, V.U., Cornell, R., Von, U., 1992. In: Cornell, R.M. (Ed.), Iron Oxides in the Laboratory. Preparation and characterization. Angewandte Chemie.
Schwertmann, U., Murad, E., 1983. Effect of pH on the formation of goethite and hematite from ferrihydrite. Clay Clay Miner. 31, 277–284. https://doi.org/10.1346/CCMN.1983.0310405.
Schwertmann, U., Friedl, J., Stanjek, H., 1999. From Fe(III) ions to ferrihydrite and then to hematite. J. Colloid Interface Sci. 209, 215–223. https://doi.org/10.1006/jcis.1998.5899.
Schwertmann, U., Stanjek, H., Becher, H.-H., 2004. Long-term in vitro transformation of 2-line ferrihydrite to goethite/hematite at 4, 10, 15 and 25°C. Clay Miner. 39, 433–438. https://doi.org/10.1180/0009855043940145.
Shaw, S., Pepper, S.E., Bryan, N.D., Livens, F.R., 2005. The kinetics and mechanisms of goethite and hematite crystallization under alkaline conditions, and in the presence of phosphate. Am. Mineral. 90, 1852–1860. https://doi.org/10.2138/am.2005.1757.
Silva, L.S., Marques Júnior, J., Barrón, V., Gomes, R.P., Teixeira, D.D.B., Siqueira, D.S., Vasconcelos, V., 2020. Spatial variability of iron oxides in soils from Brazilian sandstone and basalt. Catena 185. https://doi.org/10.1016/j.catena.2019.104258.
Smith, R.M., 2010. NIST Critically Selected Stability Constants of Metal Complexes: Version 8.0. Stand. Ref. Data Progr.
Toby, B.H., 2001. General structure analysis system - GSAS / EXPGUI, a graphical user interface for GSAS. J. Appl. Crystallogr. 34, 210–213. https://doi.org/10.1007/s10701-007-9105-0.
Vu, H.P., Shaw, S., Benning, L.G., 2008. Transformation of ferrihydrite to hematite: an in situ investigation on the kinetics and mechanisms. Mineral. Mag. 72, 217–220. https://doi.org/10.1180/minmag.2008.072.1.217.
Vu, H.P., Shaw, S., Brinza, L., Benning, L.G., 2010. Crystallization of hematite (α-Fe2O3) under alkaline condition: the effects of Pb. Cryst. Growth Des. 10, 1544–1551. https://doi.org/10.1021/cg900782g.
Walter, D., Buxbaum, G., Laqua, W., 2001. The mechanism of the thermal transformation from goethite to hematite*. J. Therm. Anal. Calorim. 63, 733–748. https://doi.org/10.1023/A:1010187921227.
Wolska, E., 1981. The structure of hydrohematite. Zeitschrift fur Krist. - New Cryst. Struct. 154, 69–75. https://doi.org/10.1524/zkri.1981.154.1-2.69.
Zhang, Y.G., Ji, J., Balsam, W.L., Liu, L., Chen, J., 2007. High resolution hematite and goethite records from ODP 1143, South China Sea: Co-evolution of monsoonal precipitation and El Niño over the past 600,000 years. Earth Planet. Sci. Lett. 264, 136–150. https://doi.org/10.1016/j.epsl.2007.09.022.